SCIENTIFIC REPORTS

OPEN

SUBJECT AREAS:
ELECTROCHEMISTRY
MATERIALS CHEMISTRY
ENERGY
SURFACE CHEMISTRY

Received
11 July 2012

Accepted
18 September 2012

Published
8 October 2012

Correspondence and requests for materials should be addressed to Y.S.-H. (shaohorn@mit.edu) or Z.L. (zliu2@lbl.gov)

* These authors contributed equally to this work.

In Situ Ambient Pressure X-ray Photoelectron Spectroscopy Studies of Lithium-Oxygen Redox Reactions

Yi-Chun Lu[1,2]*, Ethan J. Crumlin[2,3]*, Gabriel M. Veith[4], Jonathon R. Harding[2,5], Eva Mutoro[2,3], Loïc Baggetto[4], Nancy J. Dudney[4], Zhi Liu[6] & Yang Shao-Horn[1,2,3]

[1]Department of Materials Science and Engineering, [2]Electrochemical Energy Laboratory, [3]Department of Mechanical Engineering, [4]Materials Science and Technology Division, Oak Ridge National Laboratory, Oak Ridge, TN 37831, USA, [5]Department of Chemical Engineering Massachusetts Institute of Technology, Cambridge, MA 02139, USA, [6]Advanced Light Source, Lawrence Berkeley National Laboratory, Berkeley, CA 94720, USA.

The lack of fundamental understanding of the oxygen reduction and oxygen evolution in nonaqueous electrolytes significantly hinders the development of rechargeable lithium-air batteries. Here we employ a solid-state $Li_{4+x}Ti_5O_{12}$/LiPON/$Li_xV_2O_5$ cell and examine *in situ* the chemistry of Li-O_2 reaction products on $Li_xV_2O_5$ as a function of applied voltage under ultra high vacuum (UHV) and at 500 mtorr of oxygen pressure using ambient pressure X-ray photoelectron spectroscopy (APXPS). Under UHV, lithium intercalated into $Li_xV_2O_5$ while molecular oxygen was reduced to form lithium peroxide on $Li_xV_2O_5$ in the presence of oxygen upon discharge. Interestingly, the oxidation of Li_2O_2 began at much lower overpotentials (~240 mV) than the charge overpotentials of conventional Li-O_2 cells with aprotic electrolytes (~1000 mV). Our study provides the first evidence of reversible lithium peroxide formation and decomposition *in situ* on an oxide surface using a solid-state cell, and new insights into the reaction mechanism of Li-O_2 chemistry.

Electrical storage technologies are of vital importance to enable effective utilization of intermittent renewable energy sources and the creation of sustainable electric transportation. Conventional Li-ion batteries cannot meet the long-term energy storage requirements for electric vehicles, owing to their inherent gravimetric energy limitation associated with Li intercalation[1–3]. To increase gravimetric energy, one promising approach is to employ four-electron redox of oxygen, where Li-O_2 batteries have recently shown the potential to provide gravimetric energy ~4 times that of conventional Li-ion batteries[4–8]. Unfortunately, little is known about the oxygen reduction reaction (ORR) and oxygen evolution reaction (OER) mechanisms in the presence of Li^+ ions at room temperature, which has led to a number of challenges[3,5] at the oxygen electrode, limiting the practical use of this technology, such as poor round-trip efficiency[4,9], the reactivity of aprotic electrolytes with oxygen redox reaction intermediates[10], and cycle life[3]. Improving the mechanistic understanding of oxygen reduction and evolution is critical to develop strategies to overcome these challenges.

Here we study the redox of oxygen on the surface of a mixed electronic and Li^+ ionic conductor, $Li_xV_2O_5$, using a specially designed, all solid-state Li-ion battery[11], which eliminates parasitic reactions between oxygen reduction/evolution reaction intermediates and aprotic electrolytes used in conventional Li-O_2 batteries reported to date. Fourier transform infrared spectroscopy[10,12–14] and Raman spectroscopy[13,15] have shown that carbonate solvents commonly used in Li-ion batteries are not suitable for the oxygen electrode as they react with the ORR intermediate species such as the superoxide radical ion (O_2^-)[10,13], and yields parasitic reaction products such as Li_2CO_3 and lithium alkyl carbonate species. On the other hand, ether-based solvents such as dimethoxyethane (DME) are reasonably stable against O_2^- [15], where oxygen reduction leads to the formation of Li_2O_2 in first few cycles[7,16]. Unfortunately, cycling in ether-based electrolytes gradually converts Li_2O_2 to lithium carbonate-based species[16] and Li salts used in ether-based electrolytes can react with oxygen reduction products[17]. Moreover, researchers have very recently reported that carbon in the oxygen electrode can react with Li_2O_2 to form carbonates in DME[18], which increases the complexity in unraveling the Li-O_2 reaction mechanisms in aprotic electrolytes. Utilizing the special all solid-state cell design and ambient pressure X-ray photoelectron spectroscopy (APXPS)[19–21], we directly visualize the formation and disappearance of Li-O_2 reaction products (namely Li_2O_2) on an $Li_xV_2O_5$ surface *in situ* as a function of applied battery potential.

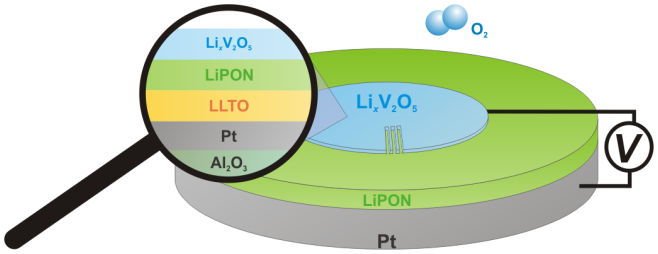

Figure 1 | Solid-state cell (LLTO/LiPON/$Li_xV_2O_5$) used for *in situ* APXPS measurements. Lithiated $Li_{4+x}Ti_5O_{12}$ (LLTO) of 750 nm supported on a Pt coated alumina disk, $Li_xV_2O_5$ of 23 nm and Li-ion conducting LiPON electrolyte of 1,000 nm were used as the negative electrode, positive electrodes, and electrolyte, respectively. LLTO was encapsulated by LiPON. XPS data were collected from the top surface of the cell, which consisted of both $Li_xV_2O_5$ and LiPON, as a function of voltage applied externally.

Results

In situ electrochemical APXPS measurements were conducted using a solid-state Li-O_2 battery[11] to probe reaction products during discharge and charge to avoid the evaporation of liquid electrolytes with low vapor pressure in the high-vacuum XPS chamber (Fig. 1). This solid-state cell consisted of lithiated lithium titanate (LLTO) as the negative electrode (having a chemical formula of $Li_{4+x}Ti_5O_{12}$)[22], lithium phosphorous oxynitride (LiPON) as the Li^+-conducting solid electrolyte (~1,000 nm thick), and vanadium oxide (V_2O_5)[23] as the positive electrode (~23 nm in thickness). The LLTO/LiPON/V_2O_5 cell was placed on a holder outfitted with electrical contacts to enable *in situ* electrochemical measurements in the XPS chamber (Supplementary Fig. S1)[24]. The Li 1s, O 1s, C 1s and V 2p spectra were collected from the top cell surface, which consisted of $Li_xV_2O_5$ and LiPON (Fig. 1), while the battery was discharged and charged potentiostatically under ultra high vacuum (UHV, pressure $< 10^{-11}$ atm) and followed by similar testing conditions in an oxygen environment at a partial pressure of $p(O_2) = 5 \times 10^{-4}$ atm (Methods and Supplementary Fig. S2). Substantial differences in the Li 1s, O 1s and V 2p spectra were observed between UHV and oxygen conditions upon charge and discharge, which will be discussed in detail below.

***In situ* XPS evidence of reversible intercalation/de-intercalation in $Li_xV_2O_5$ under UHV.** Figure 2a shows the Li 1s, O 1s and V 2p spectra as a function of potential applied across the LLTO/LiPON/$Li_xV_2O_5$ cell (V_{cell}) during discharge in UHV, where detailed information of fitted components is shown in Supplementary Table S1 and Fig. S3. We note that all the cell potentials (V_{cell}) used in this study refer to the measured open-circuit-voltage (OCV) or the applied potentials across the solid-state cell (LLTO/LiPON/$Li_xV_2O_5$). Upon discharge, the Li 1s peak position remained nearly unchanged while the peak intensity was increased slightly (up to 20% in Supplementary Fig. S3), which is due to the increasing lithium content in $Li_xV_2O_5$ as expected from Li ion migration from the LLTO to $Li_xV_2O_5$ with decreasing applied voltage from 1.8 to 0 V_{cell}. The Li 1s peak centered at 55.5 eV could be assigned to surface carbonate species such as Li_2CO_3 (55.5 eV)[25] that was formed upon air exposure on $Li_xV_2O_5$ and LiPON, $Li_xV_2O_5$ (55.7–55.9 eV)[26] and partially to LiPON (56.0 eV)[27]. The increasing Li 1s intensity was accompanied with the broadening and gradual shift of the V 2p peak to lower binding energy, indicating lowered valence state of vanadium ions upon discharge. The V 2p peak could be fitted to three peaks at 514.5 eV, 516.0 eV, and 517.4 eV, which are attributed to V^{3+}, V^{4+} and V^{5+} in $Li_xV_2O_5$, respectively[27,28]. The relative fractions of V^{3+} and V^{4+} ions were found to increase upon discharge while that of V^{5+} decreased (Supplementary Fig. S4a),

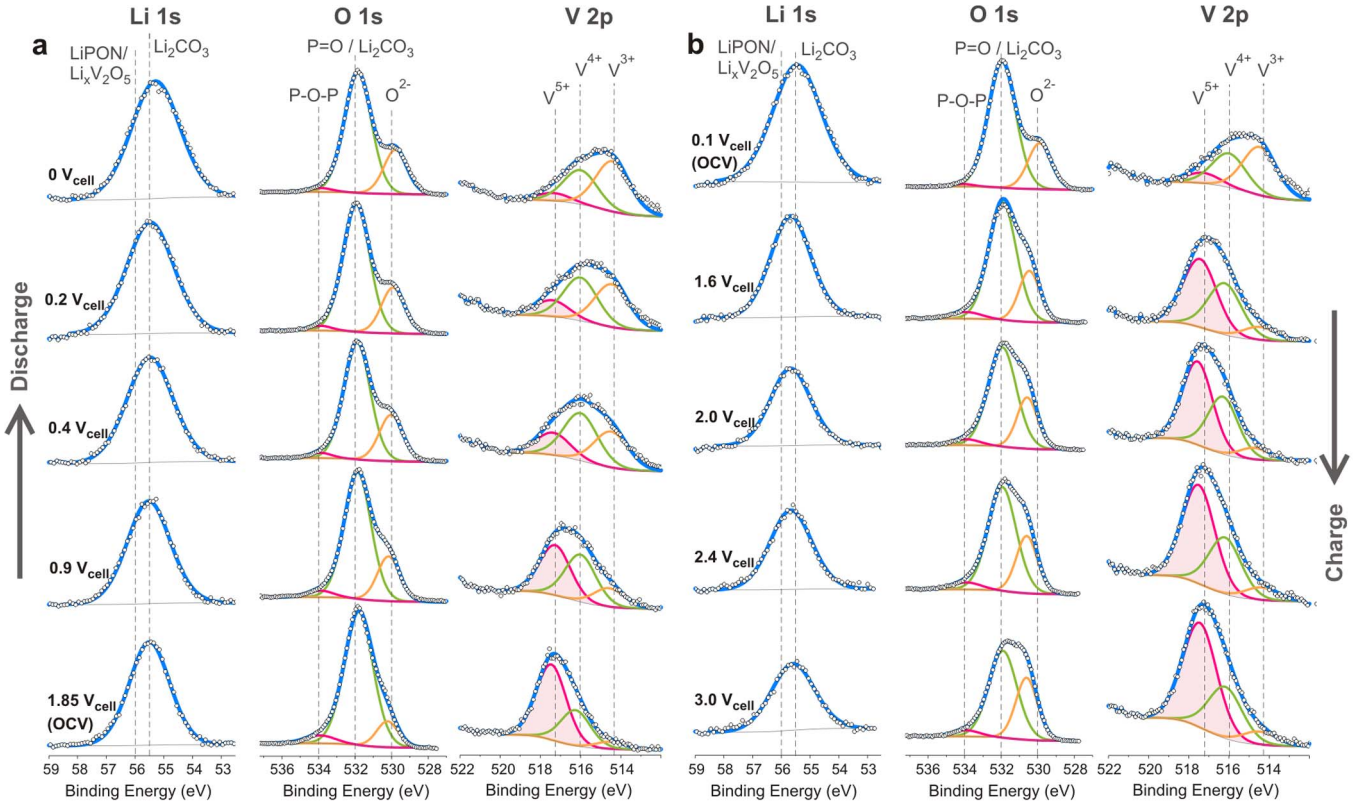

Figure 2 | *In situ* XPS data of Li 1s, O 1s, and V 2p collected under UHV. (a) Discharge from OCV (1.85 V_{cell}) to 0 V_{cell}. (b) Charge from OCV (0.1 V_{cell}) to 3.0 V_{cell}.

which was used to determine the vanadium valence state of $Li_xV_2O_5$ from 4.6+ (at 1.85 V_{cell}) to 3.6+ (at 0 V_{cell}), as shown in Fig. 3a. The changes noted in the O 1s region are in agreement with lithium intercalation into $Li_xV_2O_5$. The O 1s region includes contributions from $Li_xV_2O_5$, LiPON and surface lithium carbonate species (Li_2CO_3) formed upon air exposure of LiPON and V_2O_5 (Fig. 2a). Three components centered at 530.2, 532.0 and 534.0 eV were used to describe lattice oxygen (O^{2-}) in $Li_xV_2O_5$[27,28], both oxygen doubly bound to phosphorus (P=O)[27] and oxygen in Li_2CO_3[25], and oxygen singly bound to two phosphorus (P-O-P)[27] in LiPON, respectively. Upon discharge, the lattice oxygen (O^{2-}) in $Li_xV_2O_5$[27,28], became increasingly pronounced and led to the gradual growth of the O 1s peak shoulder at the low binding energy side. In addition, there was a systematic shift in the binding energy of the O^{2-} lattice component in $Li_xV_2O_5$ to lower binding energy by 0.4 eV from 1.85 to 0 V_{cell}, which is in agreement with decreased covalency of V-O bonds with decreasing vanadium valence state[28].

Upon charging, the changes in the Li 1s, V 2p and O 1s upon discharge were reversed, which is indicative of reversible lithium de-intercalation in $Li_xV_2O_5$, as shown in Fig. 2b. The intensity of the Li 1s region was decreased by 40% at voltages equal to and greater than 2.0 V_{cell}. (Supplementary Fig. S3). This is accompanied with increased vanadium valence state upon charging from 3.6+ (at 0.1 V_{cell}) to 4.6+ (at 3.0 V_{cell}) (Fig. 3a). It is interesting to note that the relative fractions of V^{3+}, V^{4+} and V^{5+} ions, and the covalency in the V-O bonds (having the binding energy of the O^{2-} component shifted to higher binding energy) at the end of charge (3.0 V_{cell}) were found comparable to those at the onset of discharge (1.85 V_{cell}, Supplementary Fig. S4a–b). It should be mentioned that the relative intensity of the O 1s component at 532.0 eV (assigned to Li_2CO_3 and P=O in LiPON, Fig. 2b) was considerably reduced upon charge to 3.0 V_{cell}, which suggests the decomposition of Li_2CO_3 upon charging. This hypothesis is further supported by the decreases in the C 1s component at 290.0 eV (assigned to Li_2CO_3[25] in Supplementary Fig. S5).

The vanadium valence state estimated from the XPS V 2p data as a function of applied voltage was further compared with that obtained from Li/$Li_xV_2O_5$ thin film batteries reported previously[29], as shown in Fig. 3a. Upon discharge, the vanadium valence state was changed from $V^{4.6+}$ to $V^{3.6+}$ while the valence state of vanadium was changed reversibly from $V^{3.6+}$ to $V^{4.6+}$ upon recharge. As the charge capacity (0.21 mC) was found to be larger than the discharge capacity (0.16 mC), the additional charge observed during charging can be attributed to the electrochemical oxidation of Li_2CO_3 as mentioned above. Comparable voltage profiles were noted in Fig. 3a, indicating that these *in situ* electrochemical XPS measurements in UHV showed reversible lithium intercalation in $Li_xV_2O_5$ comparable to that reported previously from Li/$Li_xV_2O_5$ thin film batteries[29].

***In situ* APXPS evidence of reversible formation and removal of Li_2O_2 on $Li_xV_2O_5$ under $p(O_2) = 5 \times 10^{-4}$ atm.** During discharge, the intensity of the Li 1s region was found to increase while that of V 2p region decreased significantly (Fig. 4a and Supplementary Fig. S6). Although the LLTO/LiPON/$Li_xV_2O_5$ cell in the presence of oxygen had a comparable discharge capacity (0.18 mC) to that in UHV (0.16 mC) (Supplementary Fig. S2), the vanadium valence state was found to decrease only slightly from 4.5+ (at 2.1 V_{cell}) to 4.25+ (at 0 V_{cell}) in Fig. 3b. The charge can be attributed largely to the formation of reaction products associated with the reduction of molecular oxygen by lithium ions on the surface of $Li_xV_2O_5$, which gradually covered the $Li_xV_2O_5$ surface upon discharge. This observation is further substantiated by the appearance and growth of a new peak centered at 531.3 eV in the O 1s region, which became dominant at the end of discharge (at 0 V_{cell}) (Fig. 4a). Considering the Li 1s binding energy shifts to 54.8 eV, this new species can be assigned to Li_2O_2 based on the binding energies of both O 1s and Li 1s peaks of a Li_2O_2 reference sample (O 1s: 531.3 eV and Li 1s: 54.7 eV)[30]. More interestingly, a minor peak centered at 528.5 eV was found to appear and grow at voltages lower than 0.2 V_{cell}, indicative of Li_2O formation (Li_2O: 528.5 eV)[31], where further studies are needed.

Upon charging, the intensity of Li 1s peak was decreased while that of V 2p was increased greatly in contrast to discharge (Fig. 4b and Supplementary Fig. S6). The charge capacity of the LLTO/LiPON/$Li_xV_2O_5$ cell in the presence of oxygen (Supplementary Fig. S2) can be attributed to not only lithium de-intercalation as evidenced by the increased vanadium valence state from 4.2+ (0.1 V_{cell}) to 4.8+ (3.0 V_{cell}) in Fig. 3b, but also the oxidation and removal of Li_2O_2 on the surface of $Li_xV_2O_5$. The latter is supported by the reduction of O 1s peak for Li_2O_2 centered at 531.3 eV and the shift of the Li 1s binding energy from 54.8 eV (Li_2O_2)[30] back to 55.5 eV (Li_2CO_3[25]/$Li_xV_2O_5$[26]/LiPON[27]). The onset of Li_2O_2 oxidation began at low applied potentials such as 1.6 V_{cell}, corresponding to voltages no greater than ~3.2 V versus Li^+/Li (V_{Li}), and Li_2O_2 was removed completely at the end of charge (3.0 V_{cell}), which re-exposed the $Li_xV_2O_5$ surface (Fig. 4b). Considering the thermodynamic reversible potential of bulk Li_2O_2 at 2.96 V_{Li}[32], the oxidation of Li_2O_2 can occur at overpotentials as low as ~0.2 V_{cell} (= 3.2 V_{Li}), which is in contrast to large charging overpotentials noted typically for Li-O_2 cells with aprotic electrolytes (~1.0 V_{cell} = 4.0 V_{Li})[33].

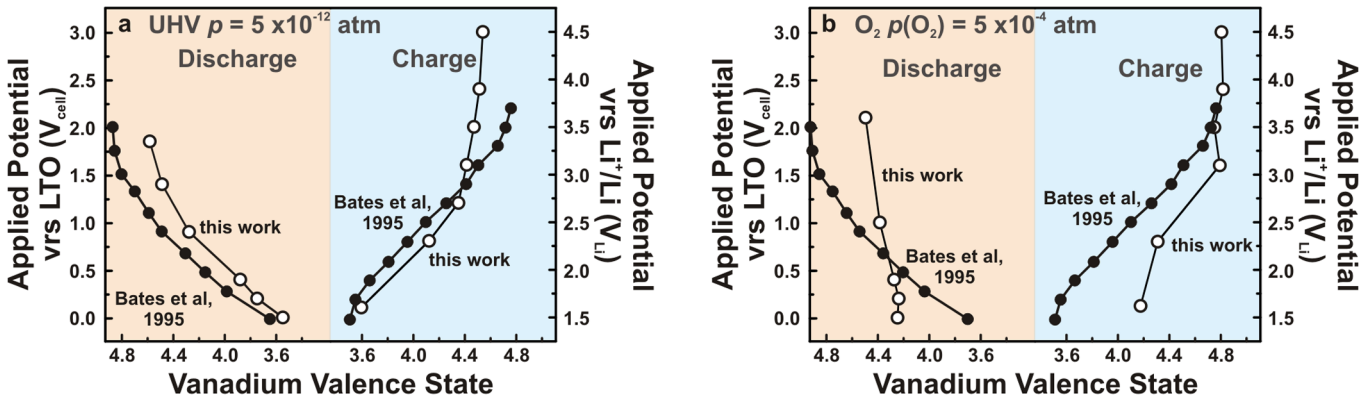

Figure 3 | $Li_xV_2O_5$ surface vanadium valence state as a function of applied voltage during cycling in UHV and $p(O_2) = 5 \times 10^{-4}$ atm. (a) The vanadium valence state of the surface of the $Li_xV_2O_5$ electrode as a function of applied voltage during discharge (left) and charge (right) under UHV. (b) The vanadium valence state of the surface of the $Li_xV_2O_5$ electrode as a function of applied voltage during discharge (left) and charge (right) under $p(O_2) = 5 \times 10^{-4}$ atm. The changes of the vanadium valence state as a function of applied potentials observed in this study (open circle) is compared with that estimated from previously reported lithium content of $Li_xV_2O_5$ from Li/$Li_xV_2O_5$ thin film batteries (solid circle)[29].

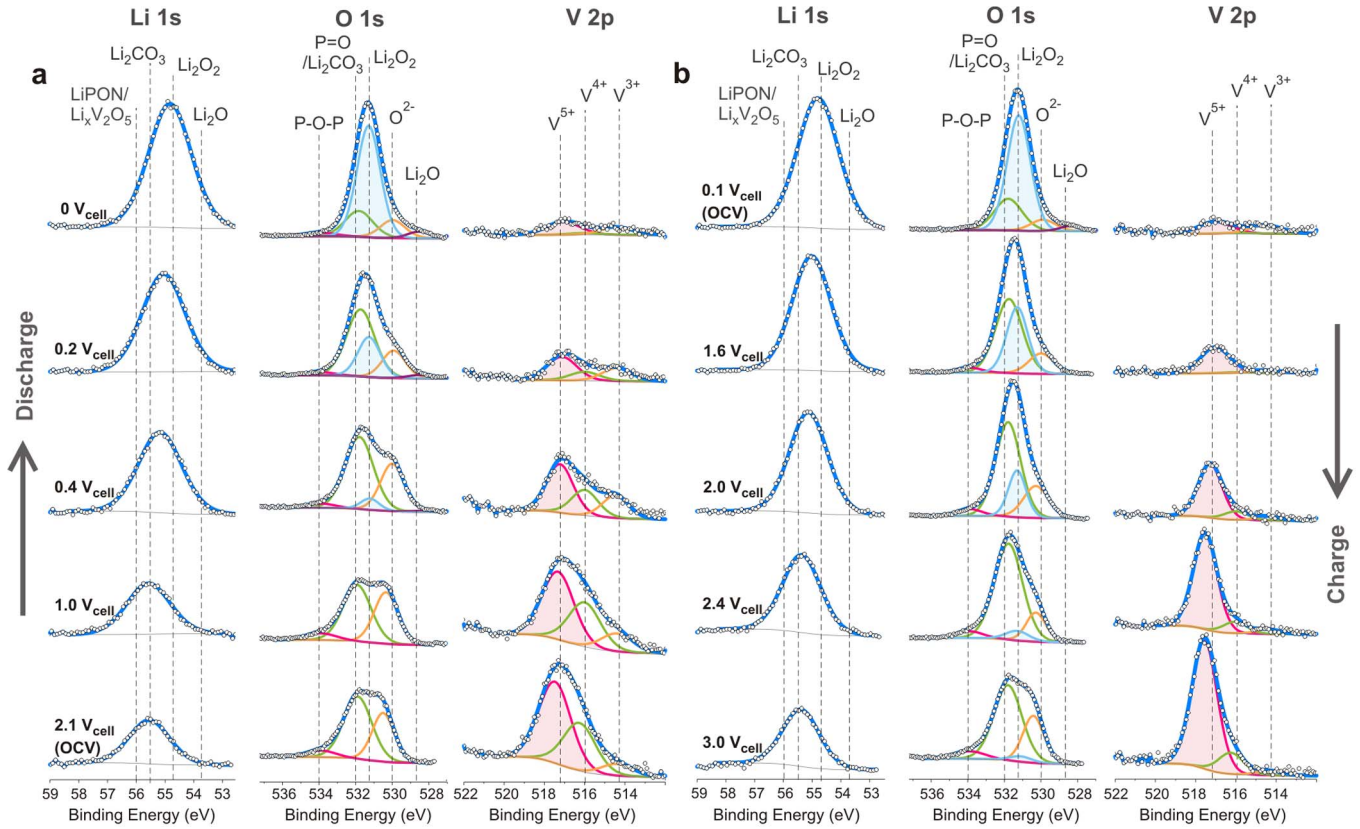

Figure 4 | ***In situ*** **APXPS data of Li 1s, O 1s, and V 2p collected under $p(O_2) = 5 \times 10^{-4}$ atm.** (a) Discharge from OCV (2.1 V_{cell}) to 0 V_{cell}. (b) Charge from OCV (0.1 V_{cell}) to 3.0 V_{cell}.

Discussion

Further studies are clearly needed to elucidate the physical origin to low overpotentials of Li_2O_2 electrochemical oxidation observed in this study. We here discuss three possibilities to highlight the differences between Li_2O_2 formed in this study and those formed in Li-O_2 batteries with aprotic electrolytes. Li_2O_2 particles formed on the surface of $Li_xV_2O_5$ are extremely thin. Considering the volumetric capacity Li_2O_2 (9716 C/cm^3) and the measured capacity associated with Li_2O_2 formed on discharge (0.71 mC/cm^2), the average thickness of maximum Li_2O_2 coverage on the $Li_xV_2O_5$ surface was estimated to be ~0.7 nm, corresponding to ~1–2 unit cells of Li_2O_2 (Supplementary Information). This is in contrast to Li_2O_2 particles having sizes in the range of 100 to 1000 nm formed in Li-O_2 batteries with aprotic electrolytes[7,33,34]. Second, the surfaces of Li_2O_2 are free of carbonate species formed on the surface of the LLTO/LiPON/$Li_xV_2O_5$ cell (no growth of the C 1s peak intensity during discharge in presence of O_2 in Supplementary Fig. S7), which is in contrast to the coverage of Li_2CO_3-like species on Li_2O_2 particles even with ether-based electrolytes[16]. Third, very thin Li_2O_2 particles may have stoichiometry and electronic properties considerably different from Li_2O_2 particles. This is supported by a recent density functional theory study reporting that the reduced coordination of oxygen atoms at the surface of Li_2O_2 yields the formation of a thin metallic region localized **at** the surface[35], which may facilitate the electro-oxidation of the Li_2O_2.

This study has, for the first time, revealed reversible oxygen reduction and evolution on an oxide surface using a solid-state lithium cell using *in situ* APXPS, as summarized in Fig. 5. Through the direct visualization of the formation and disappearance of Li-O_2 reaction products, this study connects the electrical potential to oxygen redox chemistry in presence of lithium ions at room temperature, and leads to numerous opportunities for exploiting *in situ* APXPS to gain mechanistic insights into air-based electrochemical reactions for efficient energy storage.

Methods

Negative electrode fabrication. Lithiated $Li_4Ti_5O_{12}$ (LLTO) thin film was used as the negative electrode in this study. $Li_4Ti_5O_{12}$ powder was synthesized by ball milling the stoichiometric amounts of Li_2CO_3 (Mallinckrodt – 99.5+%) and TiO_2 (Aldrich – Anatase 99.9+%), which was pressed into a 2″ diameter disk and then fired in air at

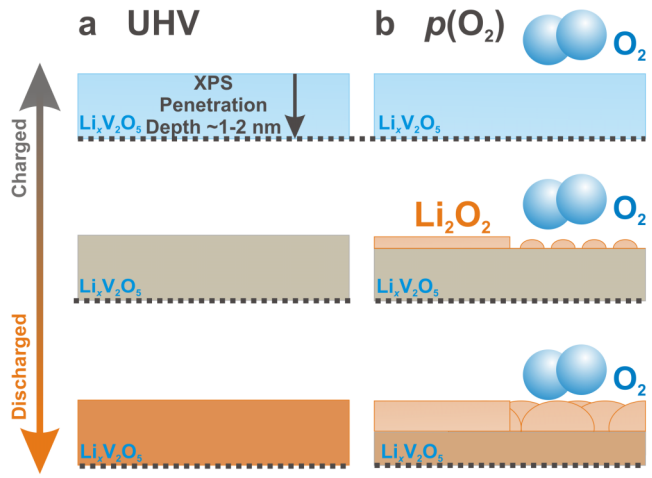

Figure 5 | **A schematic summarizing the reaction mechanism.** During discharge and charge in UHV, lithium ions reversibly intercalate/de-intercalate into/from the $Li_xV_2O_5$ electrode. During discharge in $p(O_2) = 5 \times 10^{-4}$ atm, lithium ions meet with reduced oxygen on the surface of the $Li_xV_2O_5$ electrode forming Li_2O_2, which is decomposed upon recharge in $p(O_2) = 5 \times 10^{-4}$ atm.

950°C for 10 hr. To ensure O_2 recovery upon cooling, the disk was cooled slowly at 0.5°C/min to 700°C, which was held at 700°C for 20 hr, and finally cooled down at 10°C/min to room temperature. The dense pellet was subsequently bound to a Cu plate and used as a target for magnetron sputtering. LTO films were grown by means of r.f. magnetron sputtering in an Ar atmosphere (Air Liquide – Research Grade), at an applied RF power of 80 W at a pressure of 5 mtorr, where deposition was performed once the base pressure in the chamber reached 10^{-6} torr. The films were grown on 1 cm Al_2O_3 disks (Valley Design) coated with 0.5 μm of Pt (Refining Systems, Las Vegas Nevada, USA −99.99%) on both sides, which acted as the negative electrode current collector. Sputtering of the Pt was performed in direct current mode using 25 W and 15 mtorr Ar pressure. The as-deposited LTO films with a typical thickness of 750 nm were annealed in air at 700°C for 1 hr to develop the spinel structure.

The LTO films were lithiated electrochemically in standard Swagelok cells to form $Li_7Ti_5O_{12}$[22]. The cells were prepared in an Ar filled glove box using an Li metal anode (0.75 mm Alfa Aesar −99.9%), two pieces of Celgard 2500 separator, and a few drops of 1.2 M $LiPF_6$ in ethylene carbonate/ethyl methyl carbonate electrolyte (Ferro), which was found to have water content < 2 ppm by Karl-Fisher Titration (Metler-Toledo). The cells were discharged at 5 μA current to 1.2 V using a Maccor Battery Tester. A representative discharge profile for the lithiation of the LTO films used for solid-state cells is shown in Supplementary Fig. S8, which reveals a large plateau at ~1.53 V_{Li} associated with lithium intercalation into the LTO spinel structure. The Swagelok cells were disassembled in the glove box and the lithiated LTO anodes were washed for 5 min by soaking in dimethyl carbonate (Aldrich −99% Anhydrous) to remove residual electrolyte and left to dry on filter paper in the box.

Solid electrolyte fabrication. The lithiated LTO electrodes were loaded into a vacuum chamber and pumped down until a base pressure below 3×10^{-6} torr was attained. A 1 μm thick lithium phosphorus oxynitride (LiPON) solid electrolyte layer was prepared by r.f. magnetron sputtering of a Li_3PO_4 target in a N_2 atmosphere (Air Liquide – Research Grade) at an applied power of 100 W, 20 standard cubic centimeters per minute (sccm) N_2 flow, and a pressure of 20 mtorr[11].

Positive electrode fabrication. Vanadium oxide (V_2O_5)[23] thin films were prepared by dc magnetron sputtering using a vanadium target (Kurt J. Lesker −99.9%). The films were deposited in a mixture of argon (20 sccm-Air Liquide – Research Grade) and O_2 (4 sccm-Air Liquide – Research Grade) at an applied power of 19 W and a deposition pressure of 11 mtorr. A homemade mask, cut from a stainless steel mesh, was used to add some small lines to the cathode surface. The thickness of the V_2O_5 electrode with a diameter of 0.5 cm was approximated to be 23 nm (assuming an expected deposition rate of 2.5 Å/sec for 90 seconds and on a flat surface) (corresponding to an electrode volume of $4.52 \cdot 10^{-7}$ cm^3). The solid-state cells were stored in an Ar filled glove box and shipped in sealed argon filled stainless steel vessels to the Lawrence Berkeley National Laboratories (LBNL) Advanced Light Source (ALS) for *in situ* experiments.

Experimental details of *in situ* APXPS. XPS data of Li 1s, C 1s, O 1s and V 2p were collected from the top surface of solid-state LLTO/LiPON/$Li_xV_2O_5$ cells in UHV and in presence of oxygen as a function of applied cell potential at beamline 9.3.2 at LBNL-ALS[19]. The cell was placed onto an insulating ceramic holder, where the Pt-coated cell bottom surface was in contact with a piece of Pt foil served as the negative electrode current collector. Spring-loaded Au-Pd coated tungsten tips were used to hold the cell in place and to connect the negative and positive electrodes to an external potentiostat[24]. The XPS sampling size was ~0.8 mm in diameter. No other pre-cleaning (e.g. sputtering of the surface) was carried out. XPS data were collected under the following conditions (details in Supplementary Information, Fig. S9, and S10): **a)** UHV (5×10^{-12} atm): and *open-circuit potential* (OCV) (~0.5 V_{cell}); **b)** $p(O_2) = 5 \times 10^{-4}$ atm in the cell potentials from OCV (~0.5 V_{cell}) to 0 V_{cell} and then from OCV (~0.1 V_{cell}) to 3.0 V; **c)** UHV (5×10^{-12} atm) at potentials from OCV (~2.2 V_{cell}) to 0 V_{cell}, and then OCV (~0.1 V_{cell}) to 3.0 V_{cell}; **d)** $p(O_2) = 5 \times 10^{-4}$ atm at potentials from OCV (~2.2 V_{cell}) to 0 V_{cell} upon discharge, and then from OCV (~0.1 V_{cell}) to 3.0 V_{cell}. Potentials were applied using a Bio-Logic SP-300 potenstiostat and the cell was held constant for 15 mins after each applied potential before XPS data collection at each experimental condition. XPS spectra were collected in the following sequence: low-resolution in the binding energy range from −10 to 595 eV, and then high-resolution Li 1s, O 1s, C 1s and V 2p at a photon energy of 670 eV. Data collected from steps (c) and (d) are discussed in detail in this work.

XPS data analysis. The binding energy of all the spectra was calibrated to the C 1s photoemission peak of adventitious hydrocarbons at 285.0 eV. Shirley-type background subtraction was applied to the photoemission lines, which were fitted using a combined Gaussian-Lorentzian line shape (CasaXPS). The V 2p spectra were fitted to three components (V^{3+}, V^{4+} and V^{5+}) based on the binding energy values reported previously[27,28], where all three components were constrained to have the same full-width-half-maximum (FWHM). The integrated intensity of each element and each component was extracted from the fitting, which was then normalized by its respective photo-ionization cross section. The binding energy, FWHM, and integrated peak area CasaXPS) divided by their respective photo-ionization cross section[36] (0.008985 Mbarn for Li 1s, 0.3134 Mbarn for O 1s, 1.084 Mbran for V 2p, and 0.1257 Mbarn for C 1s at 670 eV) for each component are shown in Supplementary Table S1. The cross-section normalized intensity values of Li 1s, C 1s, O 1s and V 2p as a function of applied voltage in UHV and in presence of oxygen are shown in Supplementary Fig. S11.

1. Arico, A. S., Bruce, P., Scrosati, B., Tarascon, J. M. & Van Schalkwijk, W. Nanostructured materials for advanced energy conversion and storage devices. *Nat. Mater.* **4**, 366–377 (2005).
2. Whittingham, M. S. Lithium batteries and cathode materials. *Chem. Rev.* **104**, 4271–4302 (2004).
3. Bruce, P. G., Freunberger, S. A., Hardwick, L. J. & Tarascon, J.-M. Li-O_2 and Li-S batteries with high energy storage. *Nat. Mater.* **11**, 19–29 (2012).
4. Debart, A., Paterson, A. J., Bao, J. & Bruce, P. G. α-MnO_2 nanowires: A catalyst for the O_2 electrode in rechargeable lithium batteries. *Angew. Chem.-Int. Edit.* **47**, 4521–4524 (2008).
5. Scrosati, B., Hassoun, J. & Sun, Y.-K. Lithium-ion batteries. A look into the future. *Energy Environ. Sci.* **4**, 3287–3295 (2011).
6. Lu, Y.-C., Gasteiger, H. A. & Shao-Horn, Y. Catalytic activity trends of oxygen reduction reaction for nonaqueous Li-air batteries. *J. Am. Chem. Soc.* **133**, 19048–19051 (2011).
7. Lu, Y.-C. *et al.* The discharge rate capability of rechargeable Li-O_2 batteries. *Energy Environ. Sci.* **4**, 2999–3007 (2011).
8. Jung, H.-G., Hassoun, J., Park, J.-B., Sun, Y.-K. & Scrosati, B. An improved high-performance lithium-air battery. *Nat. Chem.* **4**, 579–585 (2012).
9. Lu, Y.-C. *et al.* Platinum-gold nanoparticles: A highly active bifunctional electrocatalyst for rechargeable lithium-air batteries. *J. Am. Chem. Soc.* **132**, 12170–12171 (2010).
10. Aurbach, D., Daroux, M. L., Faguy, P. & Yeager, E. The electrochemistry of noble metal electrodes in aprotic organic solvents containing lithium salts. *J. Electroanal. Chem.* **297**, 225–244 (1991).
11. Bates, J. B., Dudney, N. J., Neudecker, B., Ueda, A. & Evans, C. D. Thin-film lithium and lithium-ion batteries. *Solid State Ion.* **135**, 33–45 (2000).
12. Mizuno, F., Nakanishi, S., Kotani, Y., Yokoishi, S. & Iba, H. Rechargeable Li-air batteries with carbonate-based liquid electrolytes. *Electrochemistry* **78**, 403–405 (2010).
13. Freunberger, S. A. *et al.* Reactions in the rechargeable lithium-O_2 battery with alkyl carbonate electrolytes. *J. Am. Chem. Soc.* **133**, 8040–8047 (2011).
14. Veith, G. M., Dudney, N. J., Howe, J. & Nanda, J. Spectroscopic characterization of solid discharge products in Li-air cells with aprotic carbonate electrolytes. *J. Phys. Chem. C* **115**, 14325–14333 (2011).
15. McCloskey, B. D., Bethune, D. S., Shelby, R. M., Girishkumar, G. & Luntz, A. C. Solvents' critical role in nonaqueous lithium-oxygen battery electrochemistry. *J. Phys. Chem. Lett.* **2**, 1161–1166 (2011).
16. Freunberger, S. A. *et al.* The lithium-oxygen battery with ether-based electrolytes. *Angew. Chem.-Int. Edit.* **50**, 8609–8613 (2011).
17. Veith, G. M., Nanda, J., Delmau, L. H. & Dudney, N. J. Influence of lithium salts on the discharge chemistry of Li-air cells. *J. Phys. Chem. Lett.* **3**, 1242–1247 (2012).
18. McCloskey, B. D. *et al.* Twin problems of interfacial carbonate formation in nonaqueous Li-O_2 batteries. *J. Phys. Chem. Lett.* **3**, 997–1001 (2012).
19. Salmeron, M. & Schlögl, R. Ambient pressure photoelectron spectroscopy: A new tool for surface science and nanotechnology. *Surf. Sci. Rep.* **63**, 169–199 (2008).
20. Crumlin, E. J. *et al.* Surface strontium enrichment on highly active perovskites for oxygen electrocatalysis in solid oxide fuel cells. *Energy Environ. Sci.* **5**, 6081–6088 (2012).
21. Zhang, C. *et al.* Measuring fundamental properties in operating solid oxide electrochemical cells by using *in situ* X-ray photoelectron spectroscopy. *Nat. Mater.* **9**, 944–949 (2010).
22. Thackeray, M. M. Structural considerations of layered and spinel lithiated oxides for lithium ion batteries. *J. Electrochem. Soc.* **142**, 2558–2563 (1995).
23. Bates, J. B. *et al.* Fabrication and characterization of amprphous lithium electrolyte thin-film batteries. *J. Power Sources* **43**, 103–110 (1993).
24. Whaley, J. A. *et al.* Note: Fixture for characterizing electrochemical devices in-operando in traditional vacuum systems. *Rev. Sci. Instrum.* **81**, 086104–086107 (2010).
25. Appapillai, A. T., Mansour, A. N., Cho, J. & Shao-Horn, Y. Microstructure of $LiCoO_2$ with and without "$AlPO_4$" nanoparticle coating: combined STEM and XPS studies. *Chem. Mat.* **19**, 5748–5757 (2007).
26. Meisel, A., Hallmeier, K. H., Szargan, R., Muller, J. & Schneider, W. Investigation of soft-Xray emission and K-edge absorption-spectra of V_2O_5 and $Li_xV_2O_5$ electrodes. *Phys. Scr.* **41**, 513–516 (1990).
27. Thißen, A. *et al.* Experimental routes to in situ characterization of the electronic structure and chemical composition of cathode materials for lithium ion batteries during lithium intercalation and deintercalation using photoelectron spectroscopy and related techniques. *Ionics* **15**, 393–403 (2009).
28. Rao, K., Pecquenard, B., Gies, A., Levasseur, A. & Etourneau, J. Structural and electrochemical behaviour of sputtered vanadium oxide films: oxygen non-stoichiometry and lithium ion sequestration. *Bull. Mat. Sci.* **29**, 535–546 (2006).
29. Bates, J. B. *et al.* Thin-film rechargeable lithium-batteries. *J. Power Sources* **54**, 58–62 (1995).
30. Yao, K. P. C. *et al.* On the thermal stability of Li_2O_2 and Li_2O for Li-Air batteries: combined XPS and XRD studies. Submitted to *J. Electrochem. Soc.* (2012).
31. Tanaka, S., Taniguchi, M. & Tanigawa, H. XPS and UPS studies on electronic structure of Li_2O. *J. Nucl. Mater.* **283**, 1405–1408 (2000).

32. Lu, Y.-C., Gasteiger, H. A., Parent, M. C., Chiloyan, V. & Shao-Horn, Y. The influence of catalysts on discharge and charge voltages of rechargeable Li-oxygen batteries. *Electrochem. Solid State Lett.* **13**, A69–A72 (2010).
33. Mitchell, R. R., Gallant, B. M., Thompson, C. V. & Shao-Horn, Y. All-carbon-nanofiber electrodes for high-energy rechargeable Li-O_2 batteries. *Energy Environ. Sci.* **4**, 2952–2958 (2011).
34. Black, R. *et al*. Screening for superoxide reactivity in Li-O_2 batteries: effect on Li_2O_2/LiOH crystallization. *J. Am. Chem. Soc.* **134**, 2902–2905 (2012).
35. Radin, M. D., Rodriguez, J. F., Tian, F. & Siegel, D. J. Lithium peroxide surfaces are metallic, while lithium oxide surfaces are not. *J. Am. Chem. Soc.* **134**, 1093–1103 (2012).
36. Yeh, J. J. & Lindau, I. Atomic subshell photoionization cross-sections and asymmetry parameters $-1 \leq Z \leq 103$. *Atom. Data Nucl. Data Tables* **32**, 1–155 (1985).

Acknowledgments

This work was supported in part by the MRSEC Program of the National Science Foundation under award number DMR- 0819762, the Assistant Secretary for Energy Efficiency and Renewable Energy, Office of FreedomCAR and Vehicle Technologies of the U. S. Department of Energy under contract no. DE-AC03-76SF00098 with the Lawrence Berkeley National Laboratory, and the Division of Materials Sciences and Engineering, Office of Basic Energy Sciences, U.S. Department of Energy. We thank Dr. Azzam Mansour (Naval Surface Warfare Center, Carderock Division) for helping with *ex situ* XPS measurements on reference materials and Rui Chang and Baohua Mao for assisting *in situ* XPS measurements. The ALS is supported by the Director, Office of Science, Office of Basic Energy Sciences, of the U.S. Department of Energy under Contract no. DE-AC02-05CH11231. Research conducted at ORNL was supported by the U.S. Department of Energy's Office of Basic Energy Science, Division of Materials Sciences and Engineering, under contract with UT-Battelle, LLC.

Author contributions

Y.-C.L. and E.J.C. contributed equally to this work. E.J.C., Y.-C.L., G.M.V. N.J.D. and Y.S.-H. designed the experiments. G.M.V., E.J.C., J.R.H. and L.B. fabricated the samples. Y.-C.L., E.J.C., E.M. and Z.L. collected the data. Y.-C.L., E.J.C. and Y.S.-H. performed the analysis. Y.-C.L., E.J.C. and Y.S.-H. wrote the manuscript and G.M.V., N.J.D., J.R.H. and Z.L. edited the manuscript.

Additional information

Supplementary information accompanies this paper at http://www.nature.com/scientificreports

Competing financial interests: The authors declare no competing financial interests.

How to cite this article: Lu, Y. *et al. In Situ* Ambient Pressure X-ray Photoelectron Spectroscopy Studies of Lithium-Oxygen Redox Reactions. *Sci. Rep.* **2**, 715; DOI:10.1038/srep00715 (2012).